The latest Application of Abaqus for the Expansion of Simulation Ability in TMC Chassis CAE

Satoshi Ito*, Phan Vinh Long*, Kouhei Shintani*,

Noriko Ohtsuka** and Izumi Kato**

*Toyota Motor Corporation

**Toyota Technical Development Corporation

Abstract: TMC Chassis CAE has used Abaqus successfully for many years.
This paper presents three recent examples of Abaqus analyses performed by TMC Chassis CAE.
1. Shape Optimization of Suspension Arm comprehending material and geometric nonlinearities.
2. A new method to identify material coefficients of static and dynamic characteristics of rubber using Abaqus. (Reproduce stress relaxing behavior, strain rate dependency, frequency dependency and amplitude dependency using one set of material coefficients)
3. FE Analysis Method to simulate the Static Stiffness Characteristic of Air Suspension Stiffness.

Keywords: Assembly Deformation, Design Optimization, Hyperelasticity, Minimum-Weight Structures, Optimization, Rubber Bushing, Suspension, Viscoelasticity.

1. Introduction

Toyota Motor Chassis CAE has used Abaqus/Standard successfully for over 20 years.

This paper presents some recent examples of Abaqus analyses performed at TMC Chassis CAE.

The first example is a numerical solution to a non-parametric shape optimization problem for the design of suspension arm. The suspension arm is evaluated by reaction force, which is the plastic buckling load due to enforced displacement. Many theses concerning shape optimization have been published, however, our approach is unique in the following point of views. First, we are using commercial software (OPTISHAPE-TS), made in Japan, for the optimization. Second, the shape optimization problem was able to consider nonlinearities by combining OPTISHAPE-TS with Abaqus.

The second example presents a new method to identify material coefficients of rubber material for static and dynamic behavior. A result about the static analysis of the suspension rubber bushing was introduced at SCC in 2010[1]. Since then, several reports have been presented regarding the dynamic characteristics analysis of rubber by using Abaqus [2]. We developed an enhanced analysis technique of the rubber bushing to expand its application to dynamic phenomena.

The third example is the simulation of the static characteristics of an Air Suspension using Abaqus. In this case, the *REBAR option is effectively used.

2. Example #1 - Shape Optimization of Suspension Arm

2.1 Comparison Between Linear Analysis and Non-linear Analysis

When a large load is applied to a Suspension Arm (See FigureA1 in Appendix), it is necessary to consider both geometrical nonlinearity and material nonlinearity to evaluate the stress distribution occurring in the component. The result of linear analysis is shown in the left side of Figure 1. It obviously differs from the result of nonlinear analysis shown on the right side of Figure 1. Therefore, it is not useful to use linear analysis for shape optimization when nonlinearity is present. However, OPTISHAPE-TS, which is the structural shape optimization commercial software that we are using, is not capable to adopt nonlinear analysis. To satisfy the requirement to include nonlinearity, we did a benchmark of other commercial shape optimization software and found that no commercial software satisfied our requirements. Therefore, we added a Plug In to OPTISHAPE-TS, which enabled the usage of Abaqus with OPTISHAPE-TS.

Figure 1. Comparison Between Linear Analysis(left) and Non- linear Analysis Results(right)

OPTISHAPE is the optimization software developed by Quint Corporation, a company located in Japan. It is capable of performing topology optimization and shape optimization as well as other commercial software. OPTISHAPE has a similar theoretical background to OPTISTRUCT, the well-known commercial software distributed by Altair Engineering. In contrast, the shape optimization was based on an original analysis method proposed by professor Azegami of Nagoya University. The details of the theory are not presented in this paper but in reference literatures such as [3].

2.2 Development of Optimization Process

Figure 2 shows a comparison between conventional process and the technique developed. Abaqus was used for the original analysis. Shape gradient is calculated by the result of the adjoint analysis. An original program was made to estimate the reaction force shown in table1. The function of commercial software was used for estimation of other cost functions. These functions are used to define the shape change limitation of the optimized area and manufacturing limitation given in the analysis model. These will be described later.

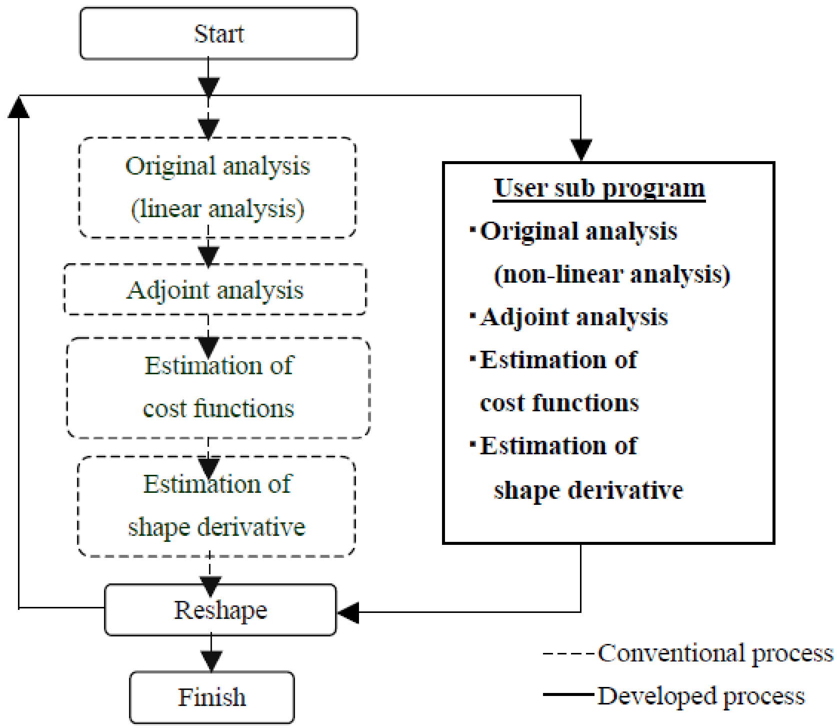

Figure 2. Comparison Between Conventional Process and Developed Process

2.3 FE Model of a Suspension Arm

Figure 3 shows the analysis model and its boundary condition. The rubber bushing (Bush) is placed at the center of the annulus ring part which is located at the right of the Suspension Arm. This part was simply modeled by using a nonlinear spring with 6 degrees of freedom. At the left of the Suspension Arm, the boundary condition of Ball Joint (BJ) is given. The enforced displacement is given at the center of the Ball Joint and the direction is indicated by the arrow shown in Figure3. The material of the suspension arm is assumed to be aluminum. The big cylinder shown at the center of Figure 3 indicates the non-design area where Coil Spring or Air Suspension ware assumed. In the part which is shown in green and red, restriction to the change of shape are defined due to the draft direction of the forging die. Also it was assumed that the reacting force of the arm generated when the enforced displacement was given to be no more than 80kN which was the target value, and the mass to be minimized during shape optimization. In addition, the target of the fatigue Safety Factor (compressive/tensile) and the average Suspension Compliance was included in the evaluation function. However, because the calculation of optimization was not able to use these values as functions of limitation, they were referred after the optimization.

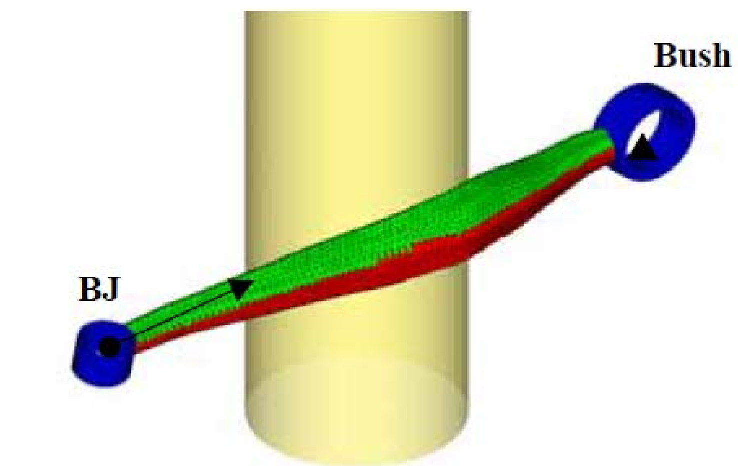

Figure 3. FE Model of Suspension Arm

2.4 Results

The numerical values of the cost functions are shown in Table 1. The mass has decreased by 130g (12%) from 1124 to 994g by the optimized calculation. The reaction force has increased to the target value of 80kN from the initial value of 58kN.

Table 1. Results of Cost Functions

	Initial	Optimum	Limit value
Mass[g]	1124	994	-
Reaction force[kN]	58	80	80 (minimum)
Compressive fatigue stress ratio[-]	0.26	0.22	1.0 (maximum)
Tensile fatigue stress ratio[-]	0.48	0.47	1.0 (maximum)
Mean compliance ratio[-]	0.18	0.12	1.0 (maximum)

Figure 4 shows the histories of each cost function with the number of shape changes. It is seen that the target of the reaction force is satisfied at the 1st shape change, and that the mass decreases afterwards. The computation time spent for nine shape changes was about 18 hours under environment of Linux(64bit), 1cpu(Intel XEON 3.6GHz), and 4GB Memory.

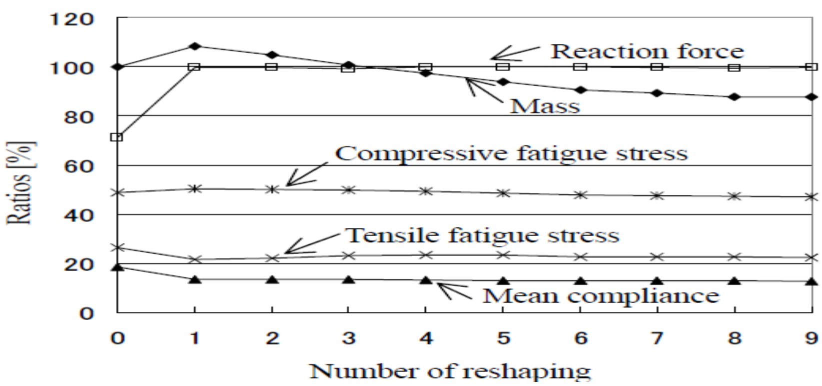

Figure 4. Variations of Cost Functions with Respect to Initial Values

Figure 5 shows the comparison of the reaction force of the optimum shape and that of the initial shape. The optimum shape satisfies the target value of 80kN. Figure 6 shows comparison of the initial shape and the optimum shape.

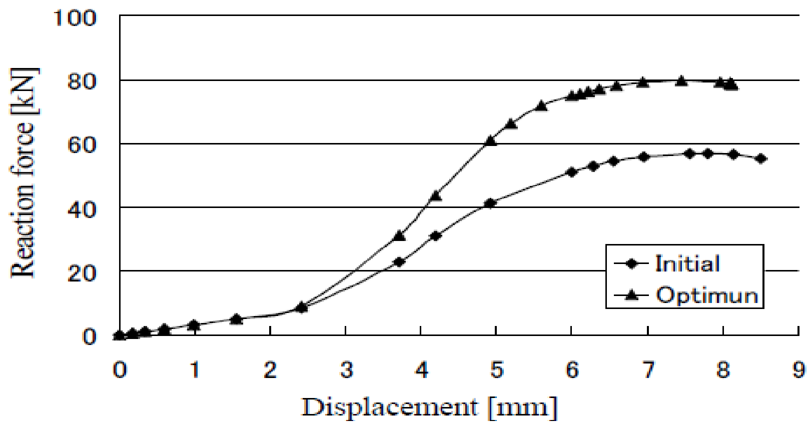

Figure 5. Relation Between Enforced Displacement and Reaction Force at center Point of BJ

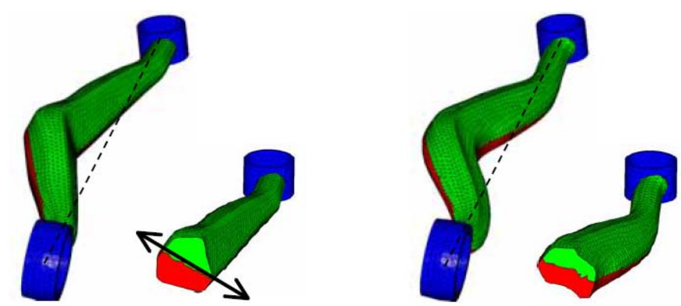

Figure 6. Initial Shape (left) and Optimum Shape (right)

It is to be understood that the optimum shape has changed at both ends of the Suspension Arm which approaches to the line of force. As a result, the bending moment decreases, and the generation of plastic deformation is avoided. The following observation can be made by studying the cross section shown in Figure 6. The arrows in the Figure indicated the direction of the transformation of the Suspension Arm. The inner of the Suspension Arm is compressed, and the outer side is pulled. This shape transformation is considered to be reasonable as the cross section of the optimum shape is close to I type arm.

The optimum shape obtained by OPTISHAPE-TS is smoother than benchmark results in other shape optimization software. The results are due to an optimization theory, named Traction Method, embedded only by OPTISHAPE-TS. By combining OPTISHAPE-TS with Abaqus, we have established an excellent structural shape optimization tool.

..

3. Example #2- A New Method to Identify Material Coefficients for Static and Dynamic Characteristics of Rubber

3.1 Material Model

The behavior of rubber shows complex static and dynamic characteristics due to stress relaxation, strain rate, frequency and amplitude dependencies. Usually it is difficult to reproduce all of rubber behaviors using standard FEM techniques. Some results, showed a possibility to represent the complex characteristics by combining material models in Abaqus, were reported [2]. However, the method requires identification of many material coefficients, usually more than ten. For matching these material coefficients, optimization tools are used, but the process seems like a black box. In this paper, we propose a new identification method for rubber which used material models in Abaqus. The proposed method uses only three material models as Figure7 below.

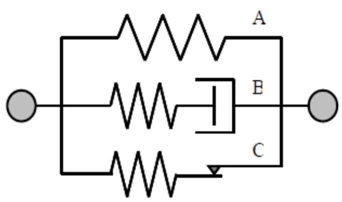

A : Hyperelasticity (*Hyperelastic)
B : Viscoelasticity (*Viscoelastic)
C : Multi-linear kinematic hardening plasticity (Built-in UMAT(MKHP))

$$\sigma = \sigma_A + \sigma_B + \sigma_C$$

Figure 7. Schematic of Material Model for Rubber

3.2 Hyperelastity

We used the Yeoh model shown by Equation (1) for hyperelasticity as described in the former report [1]. However it is originally not able to represent the dynamic characteristics due to the lack of time dependent variables.

$$U = \sum_{i=1}^{N} C_{i0}\left(\bar{I}_1 - 3\right)^i + \sum_{i=1}^{N} \frac{1}{D_i}\left(J^{el} - 1\right)^{2i} \tag{1}$$

3.3 Viscoelasticty

To represent the dynamic behavior, we add the linear viscoelastic material model of Abaqus. Equation (2) shows the dynamic modulus in the frequency domain under uniaxial harmonic vibrations. This equation can be referred from the Abaqus Analysis User's Manual [4].

$$\left|E^*\right|(\omega) = E_\infty \left\{1 + \sum_{i=1}^{N} \frac{\bar{g}_i^{\,P} \tau_i^2 \omega^2}{1 + \tau_i^2 \omega^2} \Bigg/ \left[1 - \sum_{i=1}^{N} \bar{g}_i^{\,P}\right]\right\} \Bigg/ \cos\delta \tag{2}$$

ω: Angular frequency g: Elastic modulus ratio of Prony series

τ: Relaxation time of Prony series N: Number of Prony series E_∞: Long-term elasticity

Figure 8 shows the contribution of each Prony term (g: τ) to the dynamic modulus in the frequency domain. Figure 9 shows the contribution of each Prony term (g: τ) to the relaxation ratio.

The values of (g: τ) used in each figures are show in Table2. It is clear that large g has more influence to dynamic modulus and the stress relaxation. On the other hand, the range of frequency and relaxation time in which a single value of τ influences is almost single digit. It implies that it is necessary to define multiple values of τ to represent the dynamic characteristics in wide-range frequency domain.

Since there is no variable to include the strain dependency, the amplitude dependency cannot be reproduced by using only the linear viscoelasticity model.

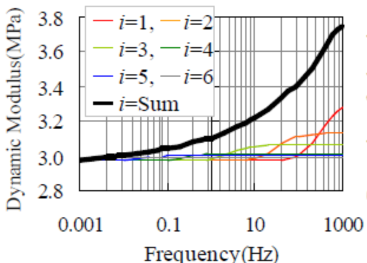

Fig.8 Frequency Dependency Behavior

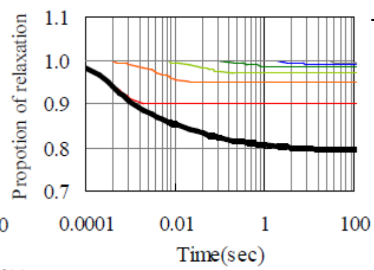

Fig.9 Stress Relaxation Behavior

Tabe2 Prony Series of viscoelasticity

i	g	τ
1	0.100	0.0005
2	0.050	0.005
3	0.030	0.05
4	0.015	0.5
5	0.010	5.0
6	0.008	50.0

3.4 Multi-linear Kinematic Hardening Plasticity

To simulate the strain amplitude dependency, a plasticity material model is added. This plasticity model is the UMAT (MKHP) model which is built-into Abaqus. The relation of stress and strain defined in the model is shown in Fig.10.The behaviors of the model under loading and unloading conditions are shown in Fig.11. The changes of gradient of the hysteresis curves when the strain at start of unloading process varies are also shown in Fig.12.

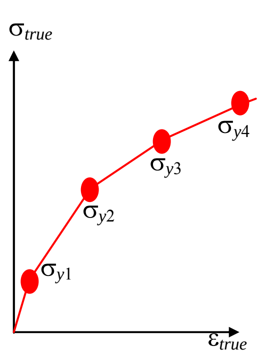

Fig.10 Material Definition of MKHP Model

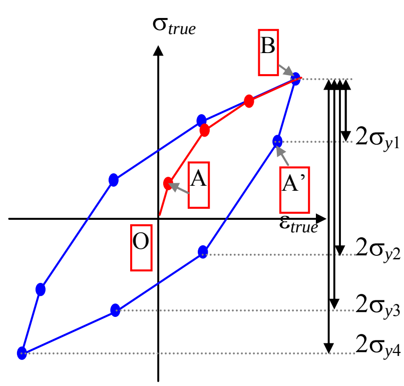

Fig.11 Material Behavior of Cyclic Load

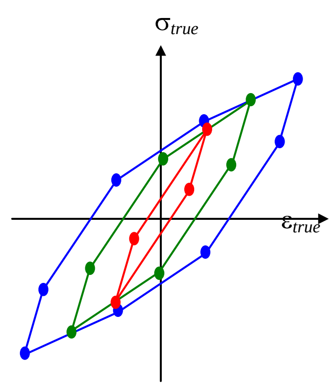

Fig.12 Dependency of the Gradient of Hysteresis Loops on Amplitude

All conclusions in 3.2-3.4 are summarized in table3.

Table 3. Targeted Material Behaviors and Related Material Model

Material behavior of identify target	Influential material model
Static	Hyperelastic, MKHP
Stress relaxation Behavior Strain rate dependency Frequency dependency	Linear- viscoelastic
Amplitude dependency	MKHP

3.5 Identify Method

It is very difficult to find the material coefficients which satisfied the demands of description of all the mechanical characteristics because the total stress in equation (1) is the sum of stress in network models at same time. By using the relations in Table 3, we developed a new procedure which identifies the material coefficients to match those characteristics which are most dominant. This procedure is implemented in a step by step process as following.

STEP1: Identify the weights of the part of the hyperelasticity, and linear viscoelasticity, and the part of the MKHP model in the absolute modulus (Figure 13).

STEP2: Identify the material coefficients of values of the MKHP model to represent the amplitude dependency.

STEP3: Indentify the material coefficient values of the hyperelasticity with the MKHP model identified in STEP2 to represent quasi static characteristics. (Figure 14).

STEP4: Identify the material coefficients values of the linear viscoelasticity so as to represent the stress-relaxation characteristics, strain-rate dependency and frequency dependency with the MKHP-model and the hyperelastic model determined in Step2 and3.

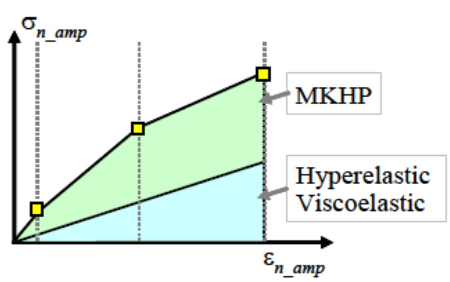

Fig.13 Restrictions to be Satisfied by the Amplitude Dependent Behavior

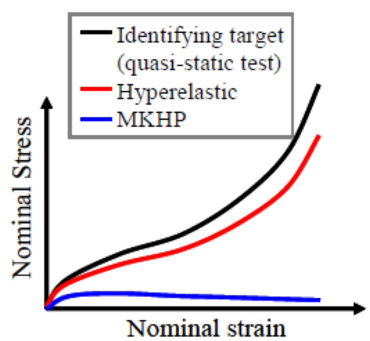

Fig.14 Restrictions to be Satisfied by the Static Behavior

3.6 Result

Simulations with using the material coefficients which are identified in previous section were performed to confirm the validity of the new method. The results are shown in Figure 15, 16 and 17. The FEA results and the experiment (TEST) results show excellent correlations.

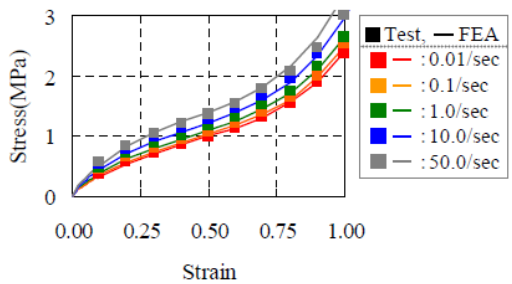

Fig.15 Constant strain rate behaviors

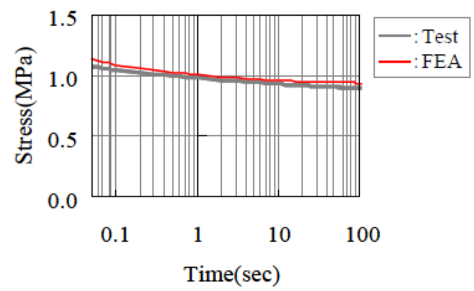

Fig.16 Stress relaxation behaviors

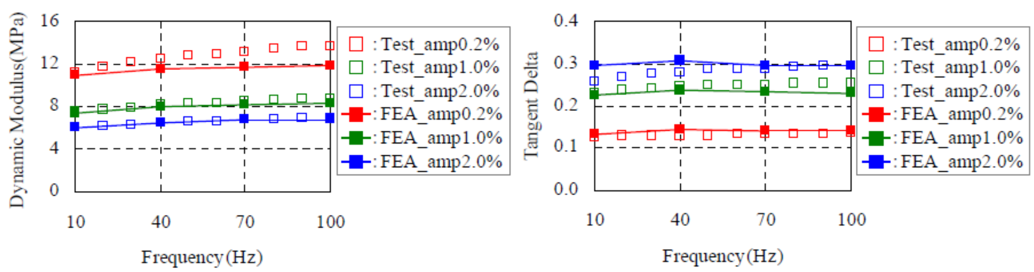

(a) Dynamic modulus (b) Tanδ

Fig.17 Frequency Domain Behaviors

4. Example #3- FE Analysis Method to Simulate Static Characteristic of Air Suspension Stiffness

4.1 Model

Figure 18 shows the configuration of a Diaphragm-type Air Spring.

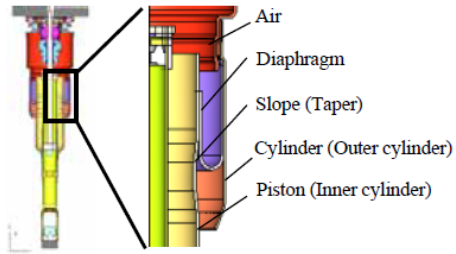

Figure 18. Configuration of Diaphragm-type Air Spring

Figure 19 shows the FE model of the Air Spring and Figure 20 shows the FE model of the diaphragm. The four layer structure of diaphragm is modeled in detail. The top and bottom rubber layer are modeled by using solid elements. The two remain cord layers are described by using *REBAR option with the cord angle is considered.

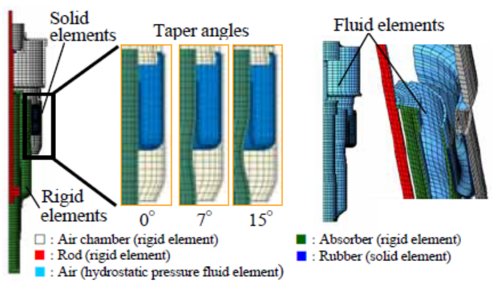

Figure 19. FE Model of Air Spring

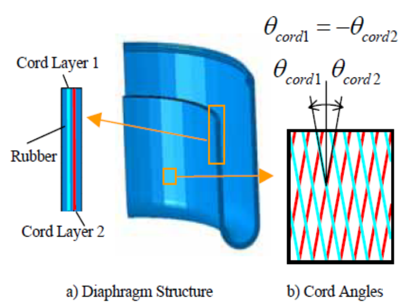

Figure 20. Diaphragm Modeling Method

4.2 Results

Figure 21 shows the simulation process. Figure 22 shows the behavior of the diaphragm during bound and rebound process of suspension when taper angle is equal to 15deg.

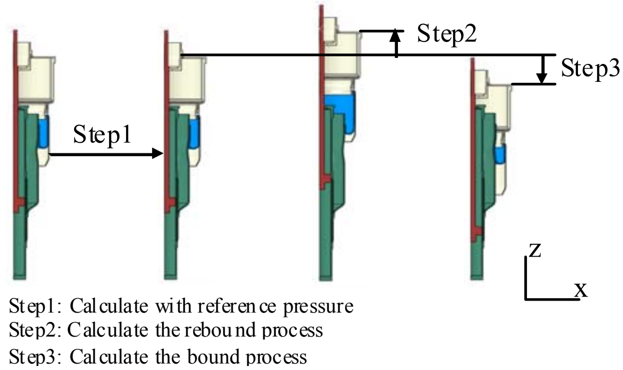

Figure 21. FE Simulation Process

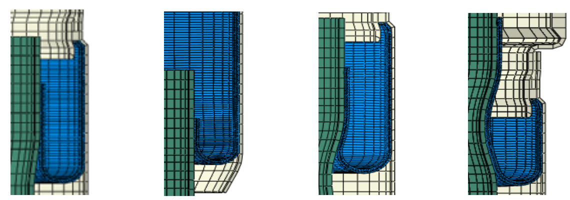

a) Initial condition b) Full rebound c) Standard d) Full bound

Figure 22. Behavior of Diaphragm During Stroke(Taper angle=15deg)

Figure 23 shows the simulation results of the Static Characteristic of the Air Springs. A poor agreement between simulation and experiment is shown in the case taper angle is equal to 15 degree. To improve the analysis accuracy we included the assembly process as shown in Figure 24.

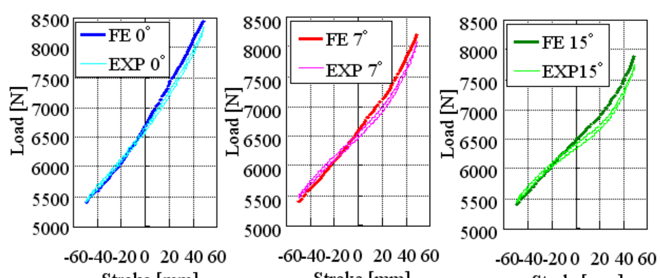

a) Taper angle 0° b) Taper angle 7° c) Taper angle 15°

Figure 23. Results of Static Characteristic of Air Springs

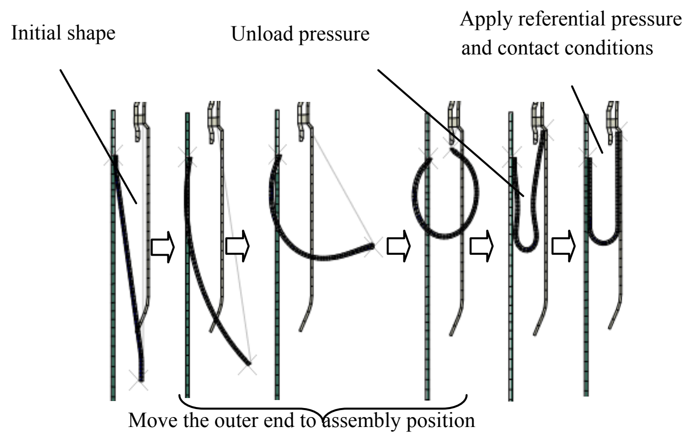

Figure 24. Simulation Step for Assembly Process of Diaphragm

Figure 25 shows the comparison between the results of the experiment and of the simulation which consider assembly process of diaphragm. The improvement of accuracy in simulation is confirmed.

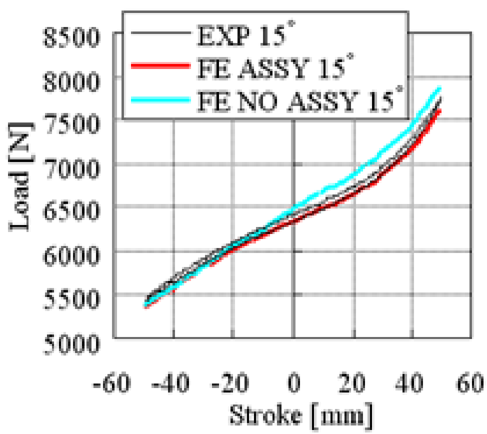

Figure 25. Results of Experiment and FE simulation

5. Conclusions

In this paper three applications of Abaqus in chassis development of TMC are presented. These application results are useful to capture some new knowledge in development of advanced suspension. With continuous improvements of its functions Abaqus will become more and more important analysis tool for chassis development at TMC.

6. References

1. Satoshi Ito, Taro Koishikura, and Diachi Suzuki, “Modeling and Analysis Techniques for Suspension Rubber Bushings”, 2010 SIMULIA Customer Conference.
2. Christopher Robert Hartley, and Jaewan Choi, “Finite Element Overlay Technique for Predicting the Payne Effect in a Filled-Rubber Cab Mount,” *SAE Int. Passeng. Cars – Mech. Syst.* , Vol. 5, Issue 1 (May 2012)
3. Azegami, H. , and Takeuchi, K. , “A Smoothing Method for Shape Optimization: Traction Method Using the Robin Condition” International Journal of Computational Methods, Vol.3, No.1, (2006) , pp.21-33
4. Abaqus Users Manual, Version 6.10-1, Dassault Systémes Simulia Corp., Providence, RI.

7. Appendix

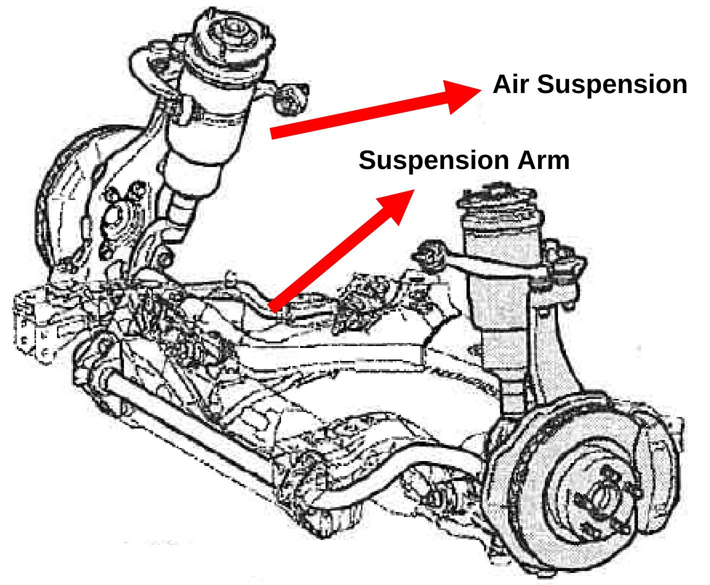

Figure A1. Front Suspension Assembly

8. Acknowledgment

The authors would like to express their gratitude to Prof.Azegami for his generous supports to the sensitivity computation in optimization.

The authors are also grateful for the support of Masataka Katayama of Dassault Systems Simulia Corp.

The authors would like to extent their sincere appreciation to everyone who helped review and correct the paper to make it better.